McCusker (1988), Cernik *et al.* (1991), Morris, Harrison, Nicol, Wilkinson & Cheetham (1992), and others.

Structures have also been solved using a two-stage method in which the integrated intensities are determined by profile fitting the individual reflections and used in a powder least-squares refinement method (*POWLS*) (Will, Bellotto, Parrish & Hart, 1988). The method was tested with silicon, which gave R(Bragg) 0.7%, and quartz, which gave 1.6%, which is a good test of the high quality of the experimental data and the profile-fitting procedure. Fig. 2.3.2.6 shows Fourier maps of orthorhombic Mg_2GeO_4 calculated using Fourier coefficients taken directly from the profile-fitting intensities.

Other types of powder studies have been carried out successfully. For example, these have been used in anomalous-scattering studies (Will, Masciocchi, Hart & Parrish, 1987; Will, Masciocchi, Parrish & Hart, 1987), Warren–Averbach profile-broadening analysis (Huang, Hart, Parrish & Masciocchi, 1987), studies of texture in thin films (Hart, Parrish & Masciocchi, 1987), and precision lattice-parameter determination (Hart, Cernik, Parrish & Toraya, 1990).

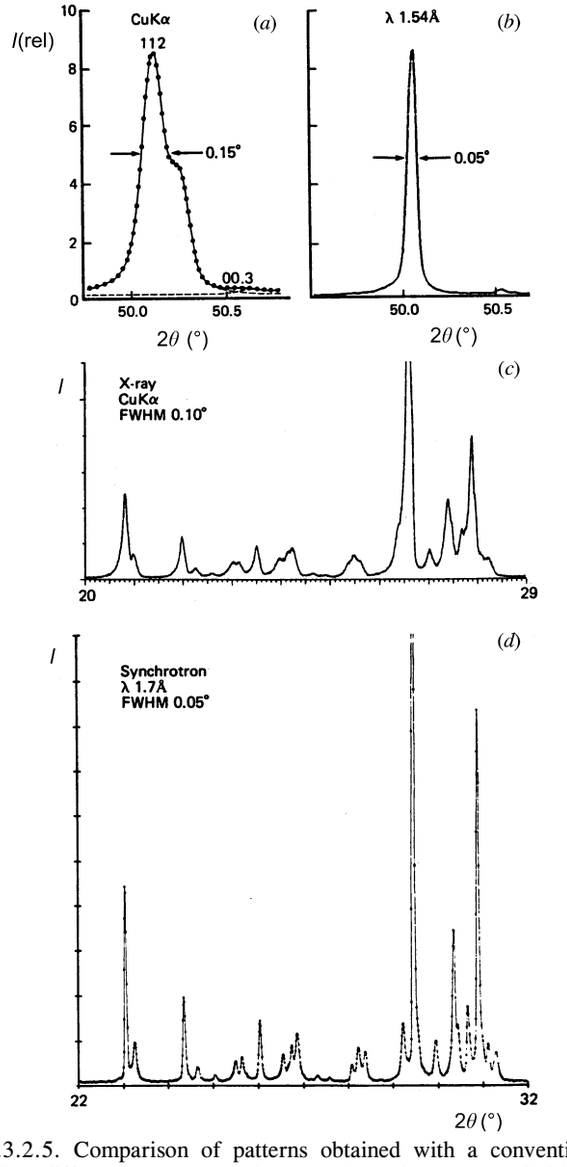

Fig. 2.3.2.5. Comparison of patterns obtained with a conventional focusing diffractometer (*a*) and (*c*), and synchrotron parallel-beam method (*b*) and (*d*). (*a*) and (*b*) quartz powder profiles; (*c*) and (*d*) mixture of equal amounts of quartz, orthoclase, and feldspar.

2.3.2.2. *Cylindrical specimen, 2θ scan*

The flat specimen can be replaced by a thin cylindrical [Fig. 2.3.2.4(*c*)] specimen as used in powder cameras. The powder can be coated on a thin fibre or reactive materials can be forced into a capillary to avoid contact with air. The intensity is lower than for flat specimens because of the smaller beam, and less powder is required. Thompson, Cox & Hastings (1987) used the method to determine the structure of Al_2O_3 by Rietveld refinement. They used a two-crystal incident-beam Si(111) monochromator; the first crystal was flat and the second a cylindrically bent triangular plate for sagittal focusing to form a 4×2 mm beam with spectral bandwidth $\Delta\lambda/\lambda \simeq 10^{-3}$.

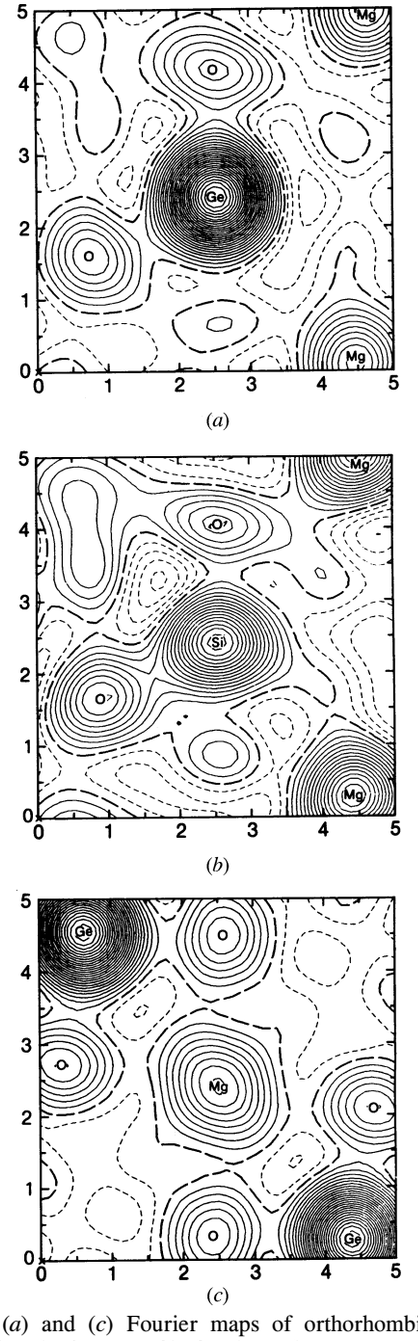

Fig. 2.3.2.6. (*a*) and (*c*) Fourier maps of orthorhombic Mg_2GeO_4 calculated directly from profile-fitted synchrotron powder data. (*b*) Fourier section of isostructural Mg_2SiO_4 calculated from single-crystal data for comparison with (*a*).

The method can also be used with a receiving slit or position-sensitive detectors (Lehmann *et al.*, 1987; Shishiguchi, Minato & Hashizume, 1986). The latter can be a short straight detector, which can be scanned to increase the data-collection speed (Göbel, 1982), or a longer curved detector.

2.3.2.3. *Grazing-incidence diffraction*

In conventional focusing geometry, the specimen and detector are coupled in θ–2θ relation at all 2θ's to avoid defocusing and profile broadening. In Seemann–Bohlin geometry, changing the specimen position necessitates realigning the diffractometer and very small incidence angles are inaccessible. In parallel-beam geometry, the specimen and detector positions can be uncoupled without loss of resolution. This freedom makes possible the use of different geometries for new applications. The specimen can be set at any angle from grazing incidence to slightly less than 2θ, and the detector scanned. Because the incident and exit angles are unequal, the relative intensities may differ by small amounts from those of the θ–2θ scan due to specimen absorption. The reflections occur from differently oriented crystallites whose planes are inclined (rather than parallel) to the specimen surface so that particle statistics becomes an important factor. The method is thus similar to Seemann–Bohlin but without focusing.

The method can be used for depth-profiling analysis of polycrystalline thin films using grazing-incidence diffraction (GID) (Lim, Parrish, Ortiz, Bellotto & Hart, 1987). If the angle of incidence θ_i is less than the critical angle of total reflection θ_c, diffraction occurs only from the top 35 to 60 Å of the film. Comparison of the GID pattern with a conventional θ–2θ pattern in which the penetration is much greater gives structural information for phase identification as a function of film depth. The intrinsic profile shapes are the same in the two patterns and broadening may indicate smaller particle sizes. However, if the film is epitaxic or highly oriented, it may not be possible to obtain a GID pattern.

For $\theta_i < \theta_c$, the penetration depth t' is (Vineyard, 1982)

$$t' \simeq \lambda/[2\pi(\theta_c^2 - \theta_i^2)^{1/2}] \qquad (2.3.2.1)$$

and, for $\theta_i > \theta_c$,

$$t' \simeq 2\theta_i/\mu, \qquad (2.3.2.2)$$

where μ is the linear absorption coefficient. The thinnest top layer of the film that can be sampled is determined by the film density, which may be less than the bulk value. As θ_i approaches θ_c, the penetration depth increases rapidly and fine control becomes more difficult. Fig. 2.3.2.7 shows this relation and the advantage of using longer wavelengths for a wider range of penetration control. For example, for a film with $\mu = 200\,\text{cm}^{-1}$, $\lambda = 1.75$ Å, and $\theta_i = 0.1°$, only the top 45 Å contribute, and increasing θ_i to 0.35° increases the depth to 130 Å. The patterns have much lower intensity than a θ–2θ scan because of the smaller diffracting volume.

Fig. 2.3.2.8 shows patterns of a 5000 Å polycrystalline film of iron oxide deposited on a glass substrate and recorded with (*a*) θ–2θ scanning and (*b*) 0.25° GID. The film has preferred orientation as shown by the numbers above the peaks in (*a*), which are the relative intensities of a random powder sample. The relative intensities are different because in (*a*) they come from planes oriented parallel to the surface and in (*b*) the planes are inclined. The glass scattering that is prominent in (*a*) is absent in (*b*) because the beam does not penetrate to the substrate.

2.3.2.4. *High-resolution energy-dispersive diffraction*

By step scanning the channel monochromator instead of the specimen, a different wavelength reaches the specimen at each step and the pattern is a plot of intensity *versus* wavelength or energy (Parrish & Hart, 1985, 1987). The X-ray optics can be the same as described in Subsection 2.3.2.1 and determines the resolution. A scintillation counter with conventional electronic circuits can be used. As in the conventional white-beam energy-

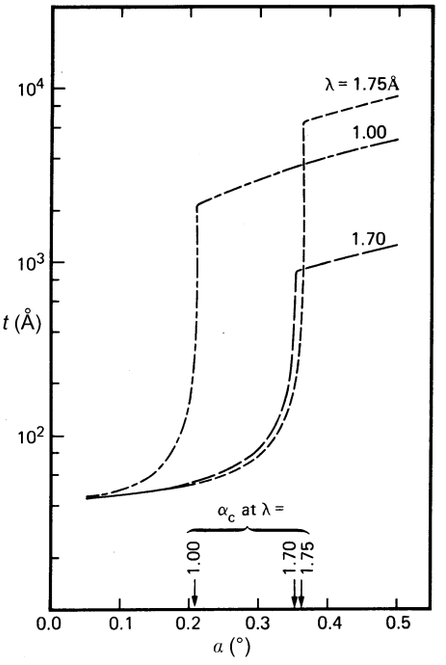

Fig. 2.3.2.7. Penetration depth t' as a function of grazing-incidence angle α for γ-Fe_2O_3 thin film. The critical angle of total reflection α_c is shown by the vertical arrows for different wavelengths.

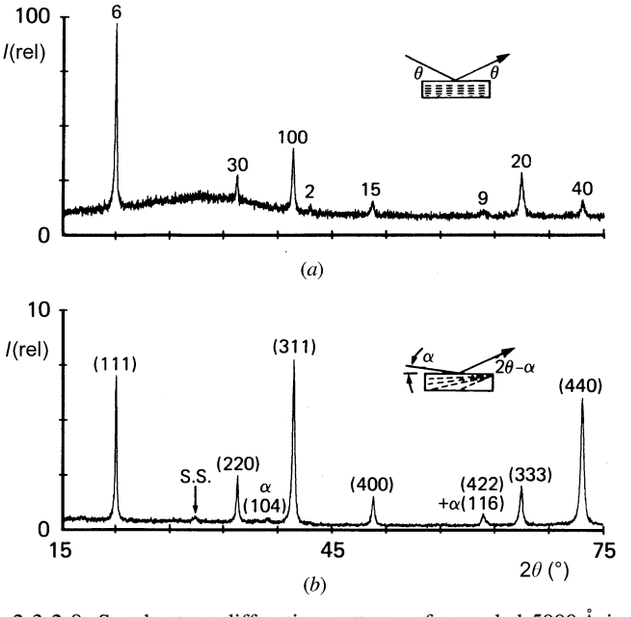

Fig. 2.3.2.8. Synchrotron diffraction patterns of annealed 5000 Å iron oxide film, $\lambda = 1.75$ Å, (*a*) θ–2θ scan; relative intensities of random powder sample shown above each reflection. (*b*) Grazing incidence pattern of same film with $\alpha = 0.25°$ showing only reflections from top 60 Å of film, superstructure peak S.S. and α-Fe_2O_3 peaks not seen in (*a*). Absolute intensity is an order of magnitude lower than (*a*).

references